Article

Benchmark Ab Initio Mapping of the F⁻ + CH₂ClI S_N2 and Proton-Abstraction Reactions

Domonkos A. Tasi,* Erik M. Orján, and Gábor Czakó*

Cite This: *J. Phys. Chem. A* 2024, 128, 10568−10578

Read Online

ACCESS | Metrics & More | Article Recommendations | Supporting Information

ABSTRACT: The experimental and theoretical studies of gas-phase S_N2 reactions have significantly broadened our understanding of the mechanisms governing even the simplest chemical processes. These investigations have not only advanced our knowledge of reaction pathways but also provided critical insights into the fundamental dynamics of chemical systems. Nevertheless, in the case of the prototypical $X^- + CH_3Y \rightarrow Y^- + CH_3X$ [X, Y = F, Cl, Br, and I] S_N2 reactions, the effect of the additional halogenation of CH_3Y has not been thoroughly explored. Thus, here, we perform the first high-level ab initio characterization of the $F^- + CH_2ClI$ S_N2 and proton-abstraction reactions utilizing the explicitly-correlated CCSD(T)-F12b method. Two possible S_N2 channels leading to the $Cl^- + CH_2FI$ and $I^- + CH_2FCl$ products are distinguished, in which we investigate four different pathways of back-side attack Walden inversion, front-side attack, double inversion, and halogen-bonded complex formation. In order to obtain the benchmark energies of the geometries of the stationary points, determined at the CCSD(T)-F12b/aug-cc-pVTZ level of theory, additional computations are carried out considering the basis set effects, post-CCSD(T) correlations, and core corrections. Using the benchmark data, we assess the accuracy of the MP2, DF-MP2, MP2-F12, and DF-MP2-F12 methods as well. By comparing the present $F^- + CH_2ClI$ system with the corresponding $F^- + CH_3Y$ [Y = Cl and I] reactions, this study demonstrates that further halogenation of CH_3Y significantly promotes the corresponding proton-abstraction and S_N2 retention channels as well as the halogen-bonded complex formation, and as a consequence, the traditional back-side attack Walden-inversion mechanism becomes less pronounced.
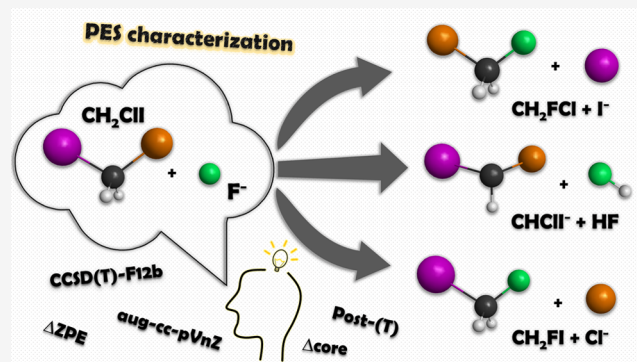
1. INTRODUCTION

The advancements in our comprehension of the fundamental bimolecular nucleophilic substitution (S_N2) reactions have substantially progressed over the last few decades.[1−6] The development of the crossed-beam velocity map imaging technique for ion−molecule reactions enabled us to study S_N2 reactions in detail;[7,8] however, utilizing theoretical methods, such as the quasi-classical trajectory (QCT) approach, remained also crucial.[9−11] With these methods at hand, the complexity of the dynamics of elemental $X^- + CH_3Y \rightarrow Y^- + CH_3X$ [X, Y = F, Cl, Br and I] S_N2 reactions has been unveiled, leading to the identification of several possible indirect and direct channels.[12−16] For the $Cl^- + CH_3I$ S_N2 reaction, a roundabout mechanism was revealed by Hase and co-workers,[7] while for $F^- + CH_3Cl$, our QCT simulations uncovered a novel indirect low-energy retention route, the so-called double-inversion pathway.[17] In the case of $F^- + CH_3I$, the formation of a H-bonded $F^-\cdots HCH_2I$ complex was found to exert a substantial influence on the S_N2 mechanism.[18] A comparative study on the $F^- + CH_3Cl/CH_3I$ S_N2 reactions was reported in order to examine the effect of the leaving Cl/I groups on the dynamics.[19] In 2023, a global analytical ab initio

potential energy surface was developed for $Cl^- + CH_3I$ to describe the dynamics of the reaction at a wide range of collision energy.[20] Moreover, the microsolvated $X^-(H_2O)_n + CH_3I$ [X = F, Cl and $n = 1 − 3$] S_N2 reactions were investigated experimentally and theoretically as well.[21−28] It is noteworthy that the stationary points of the abovementioned S_N2 reactions have also been characterized in several papers.[29−34]

On one hand, to enhance the complexity of the $X^- + CH_3Y$ S_N2 reactions, one can substitute methyl halides with different ethyl halides.[6] In these cases, bimolecular elimination (E2) can also take place competing with S_N2.[35−43] On the other hand, the impact of the halogenation on the reactions involving methyl and ethyl halides can also be considered.[6,11] However,
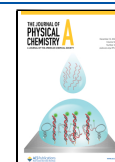
research is somewhat lacking on that matter; a small number of studies were conducted on the corresponding S_N2 and E2 reactions.[44−54] Hine and co-workers showed that additional halogenation of methyl halides results in a proportional decrease in S_N2 reactivity, correlating with the weights of the halogens.[55] Cardini and co-workers compared the $Cl^- + XCH_2Cl \rightarrow XCH_2Cl + Cl^-$ [X = H, Cl, and CN] identity S_N2 reactions by performing ab initio molecular dynamics calculations and revealed the formation of a H-bond between the reactants in the entrance channel.[51,56] A series of S_N2 reactions of halide ions and trifluoromethyl halides were analyzed by Bogdanov and McMahon concentrating on the ion−molecule complexes and transition states of the back- and front-side attack pathways, as well as of other possible mechanisms.[52] Regarding the $[I\cdots ICF_3]^-$ front-side complex of the $I^- + CF_3I$ S_N2 reaction, Verlet and co-workers reported a detailed study utilizing photoelectron spectroscopy and density functional theory.[54] Apart from the abovementioned papers, it should be also noted that reactions involving various fluorinated methyl halides were the main focus of other examinations.[49,57−59] Recently, the groups of Wester and Viggiano, in collaboration with our group, compared the $F^- + CH_3CH_2I$ and $F^- + CF_3CH_2I$ reactions to assess the influence of fluorination of the β-carbon center on the dynamics.[46]

Thus, in the present study, we report the first thorough theoretical study on the potential energy surface of the $F^- + CH_2ClI$ reaction using the high-level explicitly-correlated CCSD(T)-F12b method. Two distinct S_N2 channels resulting in the products of $Cl^- + CH_2FI$ and $I^- + CH_2FCl$ are considered; moreover, the competing proton-abstraction pathway leading to $HF + CHClI^-$ is also characterized. In the case of the S_N2 paths, several mechanisms are investigated: back-side attack, front-side attack, double inversion,[17] and halogen-bonded complex formation.[34,60] In addition, with the benchmark values in hand, we also aim to evaluate the performance of alternative lower-level ab initio methods. The current work initiates a detailed investigation of the title reaction, which is a key step toward developing a global analytical potential energy surface in order to analyze the reaction dynamics using QCT simulations. Experimental studies of the title reaction are also being conducted by the Wester group using the crossed beam ion-imaging technique. Theoretical approaches are crucial in complementing these experiments; as demonstrated in prior studies,[61,62] they yield insights beyond the reach of experimental methods. In Section 2, the computational details are described, and in Section 3, the results are presented and discussed. Finally, a summary and conclusions are provided in Section 4.

2. COMPUTATIONAL DETAILS

The stationary points of the potential energy surfaces of the $F^- + CH_2ClI$ S_N2 and proton-abstraction channels are explored by using the second-order Møller−Plesset perturbation theory (MP2) method with the augmented correlation-consistent polarized-valence-double-ζ (aug-cc-pVDZ) basis set.[63,64] Afterward, the explicitly-correlated coupled cluster singles, doubles, and perturbative triples CCSD(T)-F12b method with the aug-cc-pVnZ [n = 2 and 3] basis sets is applied to determine the structures, energies, and harmonic vibration frequencies of the stationary points.[65] The benchmark energies are computed at the CCSD(T)-F12b/aug-cc-pVTZ structures employing the CCSD(T)-F12b method with the aug-cc-pVQZ basis set, as well as considering (a) post-CCSD(T) effects and (b) core-

correlation corrections, where single-point energy computations of (a) CCSD(T),[66] CCSDT,[67] and CCSDT(Q)[68] with the aug-cc-pVDZ basis set and (b) CCSD(T)/aug-cc-pwCVTZ with both frozen-core (FC) and all-electron (AE) approaches are performed.[69] Small-core relativistic effective core potential is employed for I,[70] and the aug-cc-pVnZ-PP [n = 2−4] and aug-cc-pwCVTZ-PP basis sets are applied to replace the inner-core $1s^2\ 2s^2\ 2p^6\ 3s^2\ 3p^6\ 3d^{10}$ electrons. At the MP2/aug-cc-pVDZ level of theory, intrinsic reaction coordinate computations are also performed from the saddle points in order to provide a more in-depth characterization of the title reaction.

Hence, the benchmark classical (adiabatic) relative energies of the stationary points are obtained as

$$\Delta E(\text{CCSD(T)-F12b/aug-cc-pVQZ}) + \delta[\text{CCSDT}]$$
$$+ \delta[\text{CCSDT(Q)}] + \Delta\text{core}(+\Delta\text{ZPE}) \quad (1)$$

where

$$\delta[\text{CCSDT}] = \Delta E(\text{CCSDT/aug-cc-pVDZ})$$
$$- \Delta E(\text{CCSD(T)/aug-cc-pVDZ}) \quad (2)$$

$$\delta[\text{CCSDT(Q)}] = \Delta E(\text{CCSDT(Q)/aug-cc-pVDZ})$$
$$- \Delta E(\text{CCSDT/aug-cc-pVDZ}) \quad (3)$$

$$\Delta\text{core} = \Delta E(\text{AE-CCSD(T)/aug-cc-pwCVTZ})$$
$$- \Delta E(\text{FC-CCSD(T)/aug-cc-pwCVTZ}) \quad (4)$$

and ΔZPE is the harmonic zero-point energy correction obtained at the CCSD(T)-F12b/aug-cc-pVTZ level of theory. It is important to note that in the case of the classical energy, the nuclei are fixed at the corresponding stationary point during the calculations, meaning the energy is classical from the perspective of the nuclei, while for the adiabatic energy, it is assumed that the nuclei are in their ground vibrational state, as defined by the principles of quantum mechanics. Thus, in the case of the classical energy, the ZPE correction is not included, whereas for the adiabatic energy, which is typically presented in parentheses after the classical energy, ZPE is included. The post-CCSD(T) correction is obtained from the sum of eqs 2 and 3; however, in the present work, we examined them separately to assess the impact of each term. It should also be emphasized that, based on eqs 2 and 3, no convergence is assumed for the post-CCSD(T) corrections since the corresponding δ[CCSDT] is obtained relative to the CCSD-(T)/aug-cc-pVDZ energy, not the CCSD/aug-cc-pVDZ energy.

In the course of the assessment of the alternative MP2 methods,[71,72] the geometries and energies of the stationary points are also determined using the density-fitted DF-MP2, explicitly-correlated MP2-F12, and the corresponding DF-MP2-F12 methods with aug-cc-pVnZ [n = 2 and 3]. All the ab initio computations are carried out with the Molpro program package,[73] and for CCSDT and CCSDT(Q), the MRCC program interfaced to Molpro is employed.[74,75]

3. RESULTS AND DISCUSSION

In the case of the $F^- + CH_2ClI$ reaction, the schematic potential energy surfaces of the two possible S_N2 channels as well as of the proton-abstraction path featuring the benchmark classical (adiabatic) relative energies of the stationary points
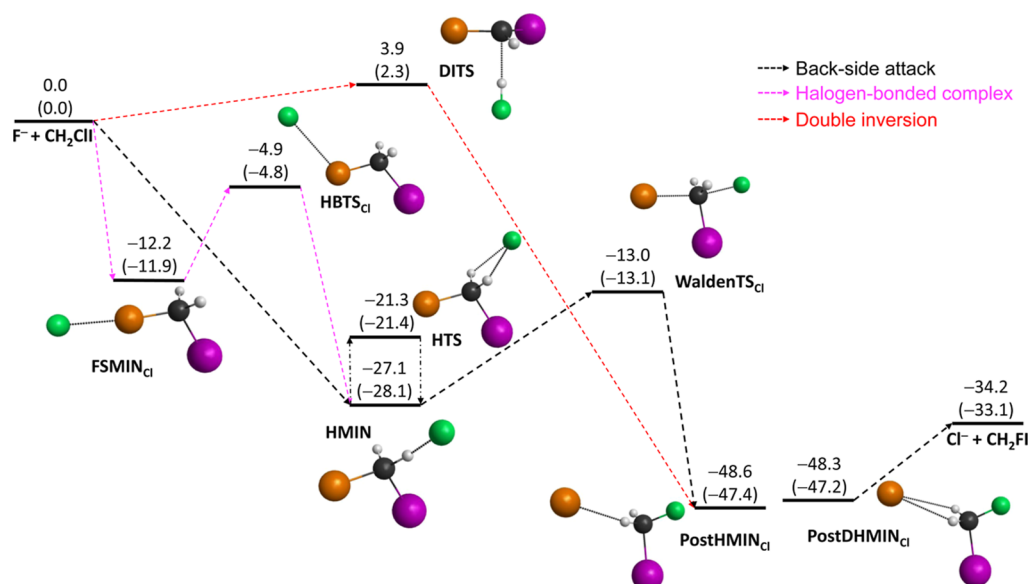
Figure 1. Schematic potential energy surface of the $F^- + CH_2ClI \rightarrow Cl^- + CH_2FI$ S_N2 reaction showing the benchmark classical (adiabatic) relative energies (kcal/mol) of the stationary points along the possible pathways. Color scheme: carbon—black, iodine—purple, chlorine—orange, fluorine—green, and hydrogen—gray.
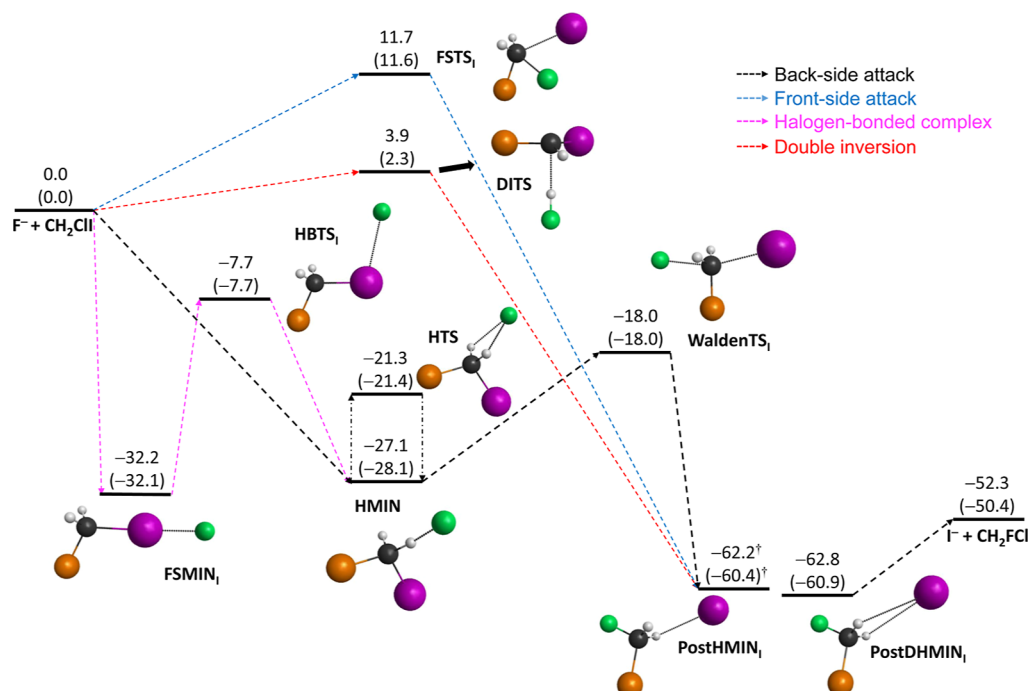

Figure 2. Schematic potential energy surface of the $F^- + CH_2ClI \rightarrow I^- + CH_2FCl$ S_N2 reaction showing the benchmark classical (adiabatic) relative energies (kcal/mol) of the stationary points along the possible pathways. Results noted with † correspond to the MP2/aug-cc-pVDZ structure. Color scheme: carbon—black, iodine—purple, chlorine—orange, fluorine—green, and hydrogen—gray.

along the possible routes are presented in Figures 1−3, respectively. Note that the corresponding stationary points are marked with "Cl" or "I", depending on the associated S_N2 channels of $Cl^- + CH_2FI$ or $I^- + CH_2FCl$ or on the viable proton-abstraction pathways. The geometries of the stationary points are depicted in Figure 4, showing the most important structural parameters. The most accurate CCSD(T)-F12b/aug-cc-pVTZ Cartesian coordinates of the complexes, transition states, reactants, and products are provided in the Supporting Information. The relative energies obtained at

different ab initio levels of theory, together with the post-CCSD(T), core, relativistic, and ZPE corrections, are given in Table 1.

As shown in Figures 1 and 2, both S_N2 channels are submerged, and since iodine is the best leaving group among the halogens, the formation of $I^- + CH_2FCl$ is more exothermic than that of the $Cl^- + CH_2FI$ products by 18.1 (17.3) kcal/mol. In the entrance region of the S_N2 channels, the same stationary points of HMIN and HTS (the H-bonded minimum and H-bonded transition state) are located.
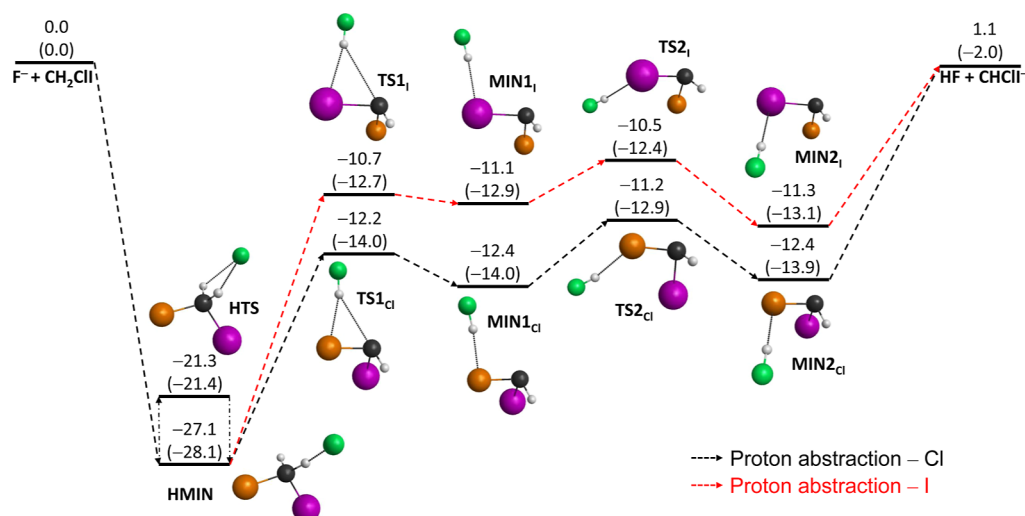
Figure 3. Schematic potential energy surface of the $F^- + CH_2ClI \rightarrow HF + CHClI^-$ proton-abstraction reaction showing the benchmark classical (adiabatic) relative energies (kcal/mol) of the stationary points along the possible pathways. Color scheme: carbon—black, iodine—purple, chlorine—orange, fluorine—green, and hydrogen—gray.

Considering the formerly characterized halogen-bonded (front-side) complex formation,[34,60] $FSMIN_I$ is situated below $FSMIN_{Cl}$ by 20.0 (20.2) kcal/mol; however, for the halogen-bonded transition states ($HBTS_{Cl}$ and $HBTS_I$), the energy difference (<3 kcal/mol) is not that significant. As seen in Figure 4, only minor differences in the structural parameters of $HBTS_{Cl}$ and $HBTS_I$ can be seen, except for the $F^-\cdots Cl-C$ and $F^-\cdots I-C$ bond angles, differing from each other by ~12°. It should also be highlighted that $FSMIN_I$ is the most stable complex in the reactant region, and no traditional $F^-\cdots H_2CClI$ ion–dipole prereaction complex can be identified. In the case of the $I^- + CH_2FCl$ S_N2 channel, the barrier height of the back-side attack mechanism is lowered by 5.0 (4.9) kcal/mol compared to the $Cl^- + CH_2FI$ channel; thus, based on the energetics of the reaction, the formation of the $I^- + CH_2FCl$ products is more favored kinetically as well as thermodynamically. The C−Cl bond at $WaldenTS_{Cl}$ is stretched by 0.388 Å and the C−I bond at $WaldenTS_I$ is lengthened by 0.306 Å, relative to the corresponding bond lengths in the CH_2ClI reactant. In the case of the C−F bonds at $WaldenTS_{Cl}$ and $WaldenTS_I$, an increase of 0.607 and 0.742 Å can be found, relative to the products of CH_2FCl and CH_2FI, in order. The global minimum of each S_N2 channel is found in the exit region with relative energies of −48.6 (−47.4) and −62.8 (−60.9) kcal/mol at the single and double H-bonded postreaction minima ($PostHMIN_{Cl}$ and $PostDHMIN_I$), respectively. Similar to the postreaction complexes of the $X^- + CH_3Y \rightarrow Y^- + CH_3X$ [Y = F, Cl, Br, and I; X = OH, NH_2, PH_2, OOH, etc.] reactions,[76-78] the dissociation energies of the leaving Cl^- at PostHMINs and PostDHMINs are larger than in the cases of I^-, and the $H\cdots Cl^-$ bonds are shortened by 0.5−0.6 Å relative to the corresponding $H\cdots I^-$ bonds. Noteworthily, based on the determined harmonic vibrational frequencies of the intermolecular modes, it is uncertain whether the $PostDHMIN_{Cl}$ and $PostDHMIN_I$ are minima or transition states. In this study, the structures identified in the product region are treated as minima. The $PostHMIN_I$ complex cannot be considered stable with complete certainty as it can be determined only at the MP2/aug-cc-pVDZ and DF-MP2/aug-cc-pVDZ levels of theory. At other levels of theory, geometry optimization results in the $PostDHMIN_I$ structure. However, in order to present a

thorough characterization of the title reaction, the corresponding $PostHMIN_I$ complex is also included in our examination. Concerning the symmetries of the aforementioned stationary points, the Cl and I variants of FSMIN, HBTS, HTS, WaldenTS, and PostDHMIN have C_s symmetry.

In a simple $X^- + CH_3Y$ S_N2 reaction, retention in the initial configuration can occur via two distinct pathways: front-side attack and double inversion. The front-side attack substitution is a direct mechanism, which goes through a high-energy transition state of $[XYCH_3]^-$. In contrast, double inversion begins with a proton abstraction by the F^-, and the system lacks sufficient energy to dissociate; therefore, HF circulates around CH_2Cl^-, subsequently forming a C−H bond and the configuration around the carbon center gets inverted. Afterward, a traditional Walden inversion takes place, which involves the formation of a C−F bond and the breaking of the C−Cl bond, resulting in retention of the initial configuration through an indirect mechanism.[17] In the case of the $I^- + CH_2FCl$ channel, the transition state ($FSTS_I$) can be identified for the front-side attack pathway with a relative energy of 11.7 (11.6) kcal/mol; however, in the alternative $Cl^- + CH_2FI$ S_N2 channel, the corresponding $FSTS_{Cl}$ cannot be determined. Relying on the structural considerations of the reactants, it can be concluded that the structure of $FSTS_{Cl}$ should be similar or even identical to that of $FSTS_I$, and differences in the lengths of the C−Cl and C−I bonds may occur; however, further theoretical and experimental investigations are necessary to validate these assumptions. The barrier of double inversion is only 3.9 (2.3) kcal/mol, and the DITS is below $FSTS_I$ by 7.7 (9.3) kcal/mol.

The schematic representation of the proton-abstraction channel of the $F^- + CH_2ClI$ reaction is depicted in Figure 3. Based on the stationary-point characterization, two different reaction pathways are proposed for proton abstraction depending on the departure of the HF product. Analogous to S_N2, each stationary point of proton abstraction is below the reactant asymptote, and with considering the ZPE corrections, the reaction turns out to be exothermic with an enthalpy of −2.0 kcal/mol. The proposed pathways are energetically distinct from each other as the Cl-labeled stationary points are located deeper than the I-labeled ones by more than 1
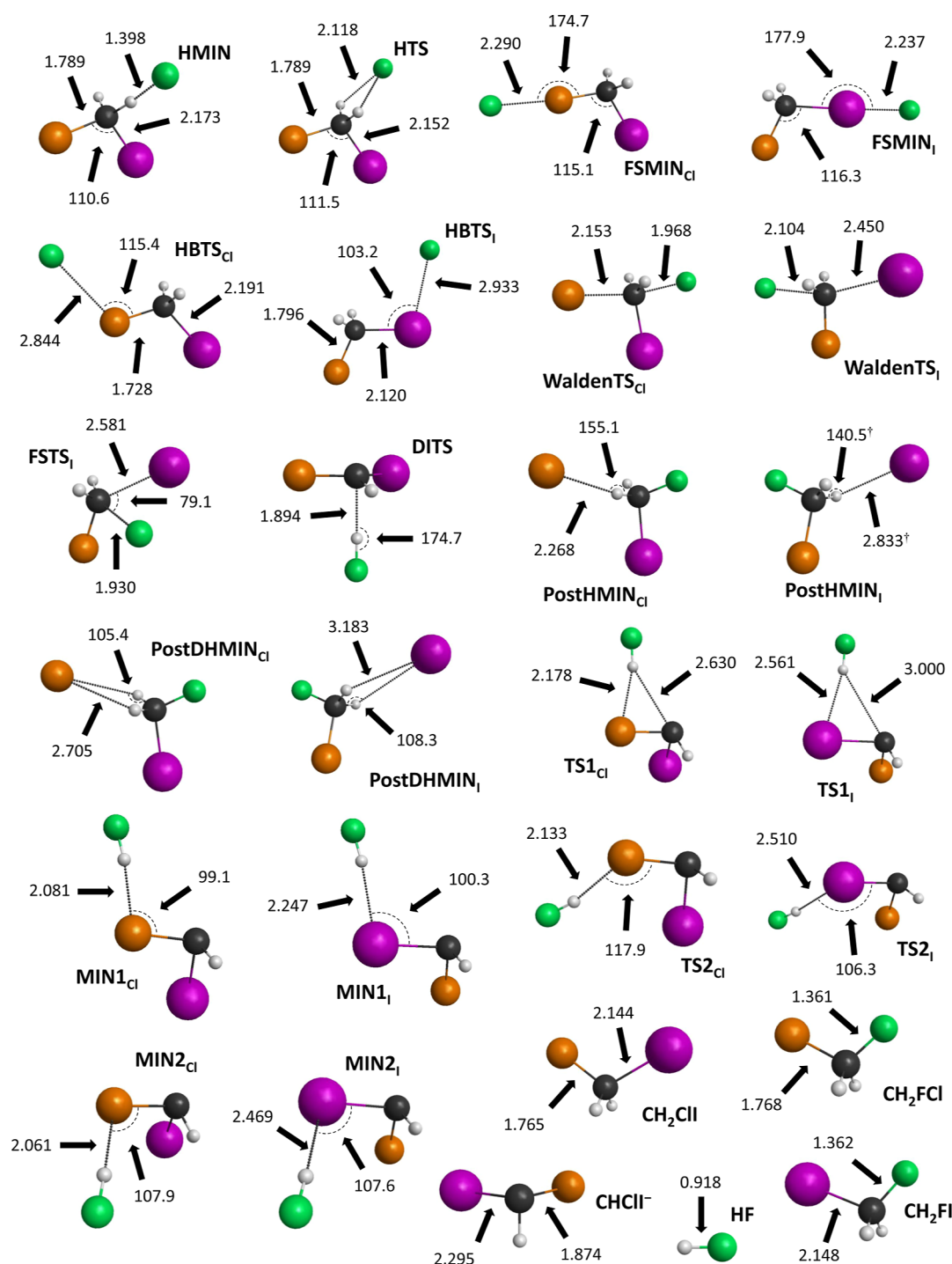
Figure 4. Most important bond lengths (Å) and angles (°) of the stationary points of the F^- + CH_2ClI S_N2 and proton-abstraction reactions obtained at the CCSD(T)-F12b/aug-cc-pVTZ level of theory. Results noted with † are obtained with MP2/aug-cc-pVDZ. Color scheme: carbon—black, iodine—purple, chlorine—orange, fluorine—green, and hydrogen—gray.

kcal/mol in each case. However, it is important to note that these two reaction pathways should not be considered completely separate as overlap between them may take place during the proton-abstraction mechanism.

In comparison to the F^- + CH_3Y [Y = Cl and I] S_N2 reactions, the replacement of a H in CH_3Y with either a Cl or I significantly changes the energetics of the potential energy surfaces.[17,32] The S_N2 channels (Cl^- + CH_2FI and I^- + CH_2FCl) of the title reaction are more exothermic than the corresponding F^- + CH_3Y → CH_3F + Y^- [Y = Cl and I]

reactions, submerged by more than 2 (Cl) and 5 (I) kcal/mol. However, the formation of the Cl^- + CH_2FI and I^- + CH_2FCl products is less preferred kinetically as the classical barriers of WaldenTS$_{Cl}$ (14.1 kcal/mol) and WaldenTS$_I$ (9.1 kcal/mol) relative to HMIN are remarkably higher than those of the transition states of $[F\cdots CH_3\cdots Cl]^-$ (3.4 kcal/mol) and $[F\cdots CH_3\cdots I]^-$ (0.2 kcal/mol). In the cases of the S_N2 retention pathways, a different situation emerges: The classical relative energy of DITS is lower than that of the transition states of the F^- + CH_3Y reactions by more than 12 [Y = Cl] and 5 [Y = I]

Table 1. Benchmark Classical and Adiabatic Relative Energies (kcal/mol) of the Stationary Points, Relative to the F⁻ + CH₂ClI Reactants, for the S_N2 and Proton-Abstraction Channels of the F⁻ + CH₂ClI Reaction

F⁻ + CH₂ClI	DZ[a]	TZ[b]	QZ[c]	δT[d]	δ(Q)[e]	Δcore[f]	classical[g]	ΔZPE[h]	adiabatic[i]
HMIN	−27.56	−27.33	−27.17	−0.02	−0.02	0.06	−27.14	−0.96	−28.11
HTS	−21.65	−21.43	−21.27	−0.04	−0.01	0.02	−21.31	−0.08	−21.38
FSMIN_Cl	−12.30	−12.22	−12.08	−0.02	−0.14	0.04	−12.20	0.31	−11.89
FSMIN_I	−32.33	−32.86	−32.82	0.05	−0.16	0.68	−32.24	0.19	−32.06
HBTS_Cl	−5.06	−4.86	−4.78	−0.05	−0.04	−0.03	−4.90	0.07	−4.83
HBTS_I	−7.25	−7.68	−7.64	−0.04	−0.03	−0.03	−7.74	0.03	−7.71
WaldenTS_Cl	−12.65	−13.17	−13.09	−0.08	−0.19	0.36	−12.99	−0.13	−13.12
WaldenTS_I	−18.14	−18.07	−18.00	−0.06	−0.23	0.25	−18.03	0.00	−18.03
FSTS_I	11.54	11.58	11.73	−0.03	−0.53	0.50	11.67	−0.08	11.58
DITS	3.60	3.66	3.76	0.11	−0.14	0.19	3.92	−1.63	2.29
PostHMIN_Cl	−48.77	−48.81	−48.82	−0.03	0.13	0.15	−48.56	1.17	−47.39
PostHMIN_I	−63.09	−62.86[j]	−63.14[j]	−0.01[j]	0.20[j]	0.74[j]	−62.21[j]	1.84[j]	−60.38[j]
PostDHMIN_Cl	−48.46	−48.55	−48.60	−0.02	0.14	0.17	−48.32	1.08	−47.23
PostDHMIN_I	−63.61	−63.40	−63.74	0.01	0.22	0.67	−62.84	1.91	−60.93
MIN1_Cl	−12.47	−12.90	−12.92	−0.05	−0.10	0.64	−12.43	−1.59	−14.03
MIN1_I	−10.97	−11.48	−11.41	−0.07	−0.10	0.47	−11.11	−1.79	−12.90
TS1_Cl	−12.33	−12.66	−12.67	−0.05	−0.10	0.61	−12.21	−1.81	−14.02
TS1_I	−10.61	−11.09	−11.03	−0.07	−0.10	0.46	−10.73	−1.99	−12.72
MIN2_Cl	−12.34	−12.83	−12.85	−0.05	−0.11	0.64	−12.38	−1.50	−13.88
MIN2_I	−11.11	−11.63	−11.56	−0.07	−0.10	0.46	−11.27	−1.79	−13.06
TS2_Cl	−11.18	−11.68	−11.71	−0.05	−0.11	0.62	−11.25	−1.67	−12.92
TS2_I	−10.40	−10.90	−10.84	−0.07	−0.10	0.48	−10.53	−1.84	−12.37
Cl⁻ + CH₂FI	−34.23	−34.48	−34.55	−0.00	0.18	0.23	−34.15	1.03	−33.12
I⁻ + CH₂FCl	−53.22	−53.03	−53.46	0.03	0.24	0.92	−52.27	1.84	−50.43
HF + CHClI⁻	1.39	0.75	0.54	−0.06	−0.09	0.74	1.13	−3.15	−2.01

[a]CCSD(T)-F12b/aug-cc-pVDZ. [b]CCSD(T)-F12b/aug-cc-pVTZ. [c]CCSD(T)-F12b/aug-cc-pVQZ relative energies at the CCSD(T)-F12b/aug-cc-pVTZ geometries. [d]CCSDT/aug-cc-pVDZ − CCSD(T)/aug-cc-pVDZ. [e]CCSDT(Q)/aug-cc-pVDZ − CCSDT/aug-cc-pVDZ. [f]AE-CCSD(T)/aug-cc-pwCVTZ − FC-CCSD(T)/aug-cc-pwCVTZ. [g]QZ + δT + δ(Q) + Δcore. [h]ΔZPE(CCSD(T)-F12b/aug-cc-pVTZ). [i]QZ + δT + δ(Q) + Δcore + ΔZPE. [j]MP2/aug-cc-pVDZ geometry and frequencies.

kcal/mol, and FSTS_I is below the front-side [FICH₃]⁻ transition state of F⁻ + CH₃I by ∼8 kcal/mol. Regarding the halogen-bonded complex formation, it should be emphasized that for F⁻ + CH₃Cl, the front-side [F···ClCH₃]⁻ complex is very weakly bound (D_e = 2.7 kcal/mol); on the contrary, the analogous FSMIN_Cl is much deeper (D_e = 12.2 kcal/mol) for the F⁻ + CH₂ClI system; moreover, a more stable FSMIN_I (D_e = 32.2 kcal/mol) is found compared to the F⁻ + CH₃I case. For the proton-abstraction channel of F⁻ + CH₂ClI, following the entrance region, the entire reaction pathway is situated over 15 kcal/mol lower than the F⁻ + CH₃I → HF + CH₂I⁻ pathway, and the corresponding HF + CHClI⁻ products are submerged by ∼20 kcal/mol compared to HF + CH₂I⁻. Furthermore, the relative barrier heights of the transition states along the proton-abstraction route are also less significant for F⁻ + CH₂ClI, and the relative barrier heights of TS1_Cl and TS1_I are comparable with the barriers of WaldenTS_Cl and WaldenTS_I. Thus, proton abstraction displays a more enhanced kinetic and thermodynamic character for the reaction studied in the present work. Taken together, these findings suggest that the additional halogenation of CH₃Y slightly hinders the probability of the traditional back-side attack Walden inversion as it significantly promotes the competing proton-abstraction channel as well as the S_N2 retention pathways and the halogen-bonded complex formation.

The classical relative energies obtained by the DF-MP2, DF-MP2-F12, MP2, and MP2-F12 methods with the aug-cc-pVDZ and aug-cc-pVTZ basis sets are summarized in Table 2. The

root-mean-square (RMS) deviations of the relative classical energies computed at the formerly mentioned levels of theory and at CCSD(T)-F12b/aug-cc-pVQZ are shown in Figure 5. In case of the complexes and transition states, the RMS values of the MP2 methods are in the range of 2.4−3.9 kcal/mol; however, for the products, higher RMS values are obtained, within 6.9−8.4 kcal/mol. Among the applied MP2 methods, the smallest RMS errors are determined for the explicitly-correlated F12 variants, and the largest differences (even >5 kcal/mol) between the relative energies provided by the non-F12 and F12 methods are obtained at DITS. The density-fitted DF-MP2 and DF-MP2-F12 methods preform nearly identically to the non-DF methods at the corresponding basis set. The most pronounced difference (0.22 kcal/mol) of the RMS values is found to be for the transition states in the case of the calculations performed at the DF-MP2-F12/aug-cc-pVDZ and MP2-F12/aug-cc-pVDZ levels of theory. As demonstrated by the RMS values of the MP2 methods, applying the aug-cc-pVTZ basis set does not substantially improve the accuracy of the relative energies compared to aug-cc-pVDZ. Therefore, the application of these MP2 methods is deemed unsuitable for the current system as they do not provide chemical accuracy for the relative energies of the stationary points. On the contrary, the RMS errors of the CCSD(T)-F12b method drop below 1 kcal/mol, reaching the values of 0.13, 0.09, and 0.49 kcal/mol at the aug-cc-pVTZ basis set for the complexes, transition states, and products, respectively. The deviations of the computed CCSD(T)-F12b energies using the aug-cc-pVnZ [n = 2 (DZ), 3 (TZ), and 4 (QZ)] basis sets are depicted in

Table 2. Classical Relative Energies (kcal/mol) of the Stationary Points, Obtained Using the DF-MP2, DF-MP2-F12, MP2, and MP2-F12 Methods with the aug-cc-pVnZ [n = 2 and 3] Basis Sets, for the S_N2 and Proton-Abstraction Channels of the F^- + CH_2ClI Reaction

basis set	aug-cc-pVDZ				aug-cc-pVTZ			
method	DF-MP2	DF-MP2-F12	MP2	MP2-F12	DF-MP2	DF-MP2-F12	MP2	MP2-F12
HMIN	−26.94	−26.91	−26.94	−26.90	−26.51	−26.60	−26.51	−26.59
HTS	−20.61	−20.91	−20.60	−20.90	−20.40	−20.54	−20.40	−20.54
FSMIN$_{Cl}$	−9.84	−11.57	−9.81	−11.54	−10.52	−11.48	−10.51	−11.47
FSMIN$_I$	−30.35	−31.59	−30.34	−31.57	−31.07	−31.98	−31.06	−31.97
HBTS$_{Cl}$	−3.73	−4.67	−3.71	−4.65	−4.13	−4.42	−4.12	−4.41
HBTS$_I$	−6.13	−6.92	−6.13	−6.92	−7.03	−7.22	−7.03	−7.22
WaldenTS$_{Cl}$	−11.93	−10.50	−11.91	−10.48	−10.86	−10.72	−10.85	−10.71
WaldenTS$_I$	−16.21	−16.07	−16.19	−16.06	−15.21	−15.75	−15.20	−15.74
FSTS$_I$	12.72	13.09	12.74	13.11	13.61	13.35	13.63	13.37
DITS	9.45	4.24	9.46	4.26	5.75	4.24	5.77	4.25
PostHMIN$_{Cl}$	−46.06	−45.33	−46.05	−45.32	−45.47	−45.08	−45.46	−45.08
PostHMIN$_I$	−58.39	−^{a}	−58.37	−^{a}	−^{a}	−^{a}	−^{a}	−^{a}
PostDHMIN$_{Cl}$	−45.62	−45.04	−45.61	−45.03	−45.01	−44.86	−45.00	−44.85
PostDHMIN$_I$	−58.41	−60.31	−58.39	−60.29	−58.54	−59.63	−58.54	−59.62
MIN1$_{Cl}$	−8.24	−8.74	−8.22	−8.72	−8.98	−9.42	−8.97	−9.41
MIN1$_I$	−6.49	−6.93	−6.47	−6.91	−7.31	−7.74	−7.30	−7.73
TS1$_{Cl}$	−8.19	−8.64	−8.16	−8.62	−8.81	−9.25	−8.80	−9.23
TS1$_I$	−6.18	−6.60	−6.15	−6.58	−6.92	−7.38	−6.90	−7.36
MIN2$_{Cl}$	−8.03	−8.61	−8.01	−8.59	−8.89	−9.34	−8.87	−9.33
MIN2$_I$	−6.61	−7.11	−6.59	−7.09	−7.48	−7.92	−7.47	−7.91
TS2$_{Cl}$	−6.81	−7.38	−6.79	−7.36	−7.66	−8.13	−7.65	−8.12
TS2$_I$	−5.80	−^{a}	−5.78	−6.31	−6.64	−7.12	−6.63	−7.11
Cl^- + CH_2FI	−31.40	−30.73	−31.39	−30.73	−30.83	−30.68	−30.83	−30.68
I^- + CH_2FCl	−47.62	−49.89	−47.59	−49.86	−47.91	−49.16	−47.90	−49.15
HF + $CHClI^-$	5.54	5.32	5.56	5.34	5.15	4.36	5.16	4.37

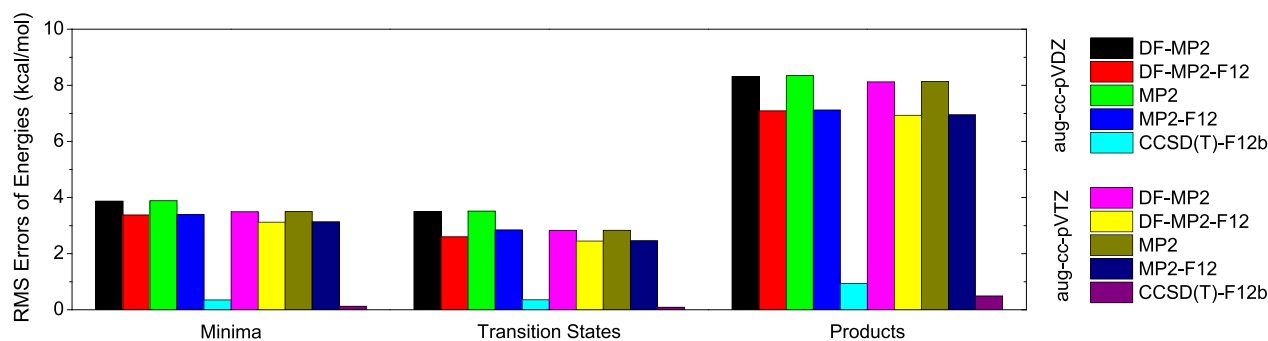^{a}Geometry optimization does not converge.

Figure 5. RMS errors of the classical energies of the complexes (minima), transition states, and products obtained at various levels of theory relative to the CCSD(T)-F12b/aug-cc-pVQZ values in the case of the F^- + CH_2ClI S_N2 and proton-abstraction reactions.
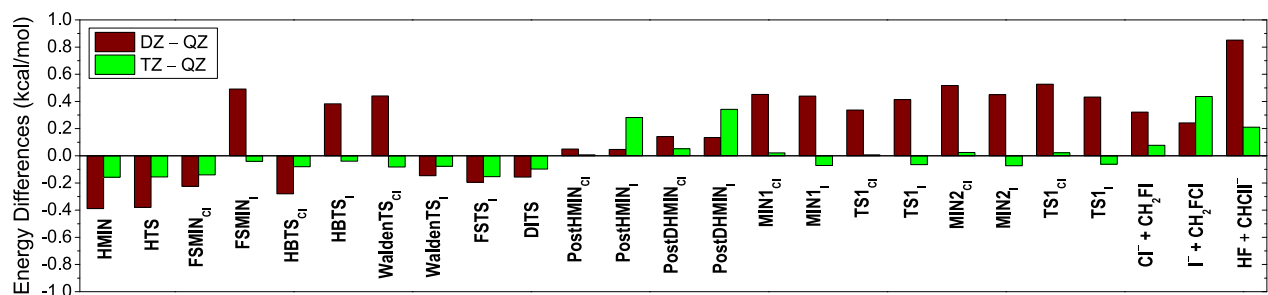

Figure 6. Basis-set convergence of the CCSD(T)-F12b relative energies using the aug-cc-pVDZ (DZ), aug-cc-pVTZ (TZ), and aug-cc-pVQZ (QZ) basis sets for the stationary points of the S_N2 and proton-abstraction channels of the F^- + CH_2ClI reaction.

Figure 6; also, the post-CCSD(T) and the core correlations, obtained from eqs 2−4, are shown for the stationary points of

the F^- + CH_2ClI reaction in Figure 7. As expected, the explicitly-correlated CCSD(T)-F12b method displays a fast
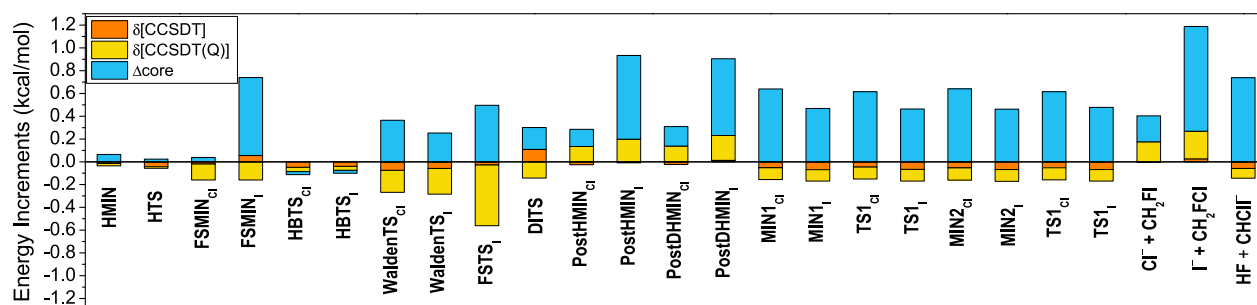
Figure 7. Post-CCSD(T), eqs 2 and 3, and core correlation, eq 4, energy effects for the stationary points of the F⁻ + CH$_2$ClI S$_N$2 and proton-abstraction reactions.

basis-set convergence: typically, the DZ versus QZ differences are within ±0.55 kcal/mol, while the deviations of TZ and QZ are within ±0.20 kcal/mol. The largest difference (0.85 kcal/mol) can be identified for the HF + CHClI⁻ products; moreover, in the case of PostHMIN$_I$, PostDHMIN$_I$, and I⁻ + CH$_2$FCl, the basis-set convergence breaks as the obtained TZ−QZ is higher than the corresponding DZ−QZ by 0.23, 0.21, and 0.19 kcal/mol, respectively. As seen in Figure 7, core corrections usually have an opposite sign to the post-CCSD(T) effects, thereby reducing their combined impact and resulting in energy contributions within the 0.3−0.6 kcal/mol range. However, there are instances when their effects are cumulative: significant auxiliary energy contributions of 1.2 and 0.9 kcal/mol are determined for the I⁻ + CH$_2$FCl products and the PostDHMIN$_I$ complex, signifying the importance of their consideration. The ZPE corrections of the stationary points obtained at the CCSD(T)-F12b/aug-cc-pVTZ level of theory are presented in Table 1. As it can be seen, for the FSMIN$_{Cl}$, FSMIN$_I$, PostHMIN$_{Cl}$, PostHMIN$_I$, PostDHMIN$_{Cl}$, Post-DHMIN$_I$ complexes and the HBTS$_{Cl}$ and HBTS$_I$ transition states as well as for the Cl⁻ + CH$_2$FI and I⁻ + CH$_2$FCl products, positive ΔZPEs can be determined, which increase the energy levels of the stationary points and decrease the exothermicity of the S$_N$2 channels. In almost every case, the ZPE effects are within ±2.0 kcal/mol, except for the HF + CHClI⁻ products, where a substantial value of −3.15 kcal/mol is observed. Similarly, in the cases of the Cl⁻ + CH$_2$FI and I⁻ + CH$_2$FCl S$_N$2 products, noticeable ZPE corrections of 1.03 and 1.84 kcal/mol can be recognized, demonstrating that the consideration of these ZPE corrections, along with the core and post-CCSD(T) effects, is required in order to achieve accurate reaction enthalpies.

4. SUMMARY AND CONCLUSIONS

In this work, we investigated the potential energy surfaces of the S$_N$2 and proton-abstraction channels of the F⁻ + CH$_2$ClI reaction using the explicitly-correlated CCSD(T)-F12b method with the aug-cc-pVnZ [n = 2 and 3] basis sets. Since there are two possible halide ions (Cl⁻ and I⁻) that can act as a leaving group in the S$_N$2 process, we have characterized two distinct S$_N$2 pathways leading to the Cl⁻ + CH$_2$FI and I⁻ + CH$_2$FCl products. It was verified that the formation of I⁻ + CH$_2$FCl is thermodynamically more favored than that of Cl⁻ + CH$_2$FI. Within each S$_N$2 channel, four distinct pathways have been considered: back-side attack, front-side attack, double inversion,[17] and halogen-bonded complex formation.[34,60] In the entrance region of the I⁻ + CH$_2$FCl S$_N$2 channel, stable front-side complex formation has been unveiled as the corresponding [F···IClCH$_2$]⁻ complex is located below the

reactant asymptote by an enormous classical (adiabatic) energy of 32.2 (32.1) kcal/mol. Regarding the S$_N$2 retention pathways, the barrier height of the front-side attack path of the I⁻ + CH$_2$FCl S$_N$2 channel is situated above that of double inversion by 7.7 (9.3) kcal/mol; however, no front-side transition state can be identified in the case of the Cl⁻ + CH$_2$FI channel. Moreover, the comparison with the conventional F⁻ + CH$_3$Y [Y = Cl and I] S$_N$2 reactions[17,32] uncovered that the additional halogenation of CH$_3$Y causes a somewhat less preferred back-side attack Walden-inversion pathway since it enhances the prevalence of the proton-abstraction and S$_N$2 retention channels as well as of the halogen-bonded complex formation. However, it should be emphasized that these findings, derived from the energy profiles of the possible pathways, await validation through subsequent theoretical and experimental examinations on the dynamics of the title reaction. The basis-set convergence of the CCSD(T)-F12b methods, as well as the ZPE contributions and the auxiliary energy corrections of post-CCSD(T) and core correlations, have also been investigated. Furthermore, the stationary points have been characterized by utilizing the MP2, DF-MP2, MP2-F12, and DF-MP2-F12 methods in order to test the performance of different ab initio levels of theory for the F⁻ + CH$_2$ClI system.

Overall, the present study highlights the incomplete understanding of even basic S$_N$2 reactions involving additionally halogenated substrate molecules; therefore, we expect that this work will pave the way for further comprehensive experimental and theoretical examinations of such reactions.

■ ASSOCIATED CONTENT

Ⓢ Supporting Information

The Supporting Information is available free of charge at https://pubs.acs.org/doi/10.1021/acs.jpca.4c06716.

> Benchmark Cartesian coordinates (Å) and energies (E_h) of the stationary points (PDF)

■ AUTHOR INFORMATION

Corresponding Authors

Domonkos A. Tasi − *MTA-SZTE Lendület "Momentum" Computational Reaction Dynamics Research Group, Interdisciplinary Excellence Centre and Department of Physical Chemistry and Materials Science, Institute of Chemistry, University of Szeged, Szeged H-6720, Hungary;* Present Address: Lehrstuhl für Theoretische Chemie, Ruhr-Universität Bochum, 44780 Bochum, Germany; ⦿ orcid.org/0000-0002-9751-0802; Email: dtasi@chem.u-szeged.hu

Gábor Czakó − *MTA-SZTE Lendület "Momentum" Computational Reaction Dynamics Research Group, Interdisciplinary Excellence Centre and Department of Physical Chemistry and Materials Science, Institute of Chemistry, University of Szeged, Szeged H-6720, Hungary;* orcid.org/0000-0001-5136-4777; Email: gczako@chem.u-szeged.hu

Author

Erik M. Orján − *MTA-SZTE Lendület "Momentum" Computational Reaction Dynamics Research Group, Interdisciplinary Excellence Centre and Department of Physical Chemistry and Materials Science, Institute of Chemistry, University of Szeged, Szeged H-6720, Hungary;* Present Address: Department of Pathophysiology, University of Szeged, Semmelweis u. 1, 6725 Szeged, Hungary; orcid.org/0000-0003-4176-0834

Complete contact information is available at:
https://pubs.acs.org/10.1021/acs.jpca.4c06716

Notes
The authors declare no competing financial interest.

■ ACKNOWLEDGMENTS

■ REFERENCES

(1) Shaik, S. S.; Schlegel, H. B.; Wolfe, S. *Theoretical Aspects of Physical Organic Chemistry: The S_N2 Mechanism*; Wiley: New York, 1992.

(2) Hase, W. L. Simulations of Gas-Phase Chemical Reactions: Applications to S_N2 Nucleophilic Substitution. *Science* **1994**, *266*, 998−1002.

(3) Chabinyc, M. L.; Craig, S. L.; Regan, C. K.; Brauman, J. I. Gas-Phase Ionic Reactions: Dynamics and Mechanism of Nucleophilic Displacements. *Science* **1998**, *279*, 1882−1886.

(4) Laerdahl, J. K.; Uggerud, E. Gas Phase Nucleophilic Substitution. *Int. J. Mass Spectrom.* **2002**, *214*, 277−314.

(5) Uggerud, E. The Factors Determining Reactivity in Nucleophilic Substitution. *Adv. Phys. Org. Chem.* **2017**, *51*, 1−57.

(6) Hamlin, T. A.; Swart, M.; Bickelhaupt, F. M. Nucleophilic Substitution (S_N2): Dependence on Nucleophile, Leaving Group, Central Atom, Substituents, and Solvent. *ChemPhysChem* **2018**, *19*, 1315−1330.

(7) Mikosch, J.; Trippel, S.; Eichhorn, C.; Otto, R.; Lourderaj, U.; Zhang, J. X.; Hase, W. L.; Weidemüller, M.; Wester, R. Imaging Nucleophilic Substitution Dynamics. *Science* **2008**, *319*, 183−186.

(8) Meyer, J.; Wester, R. Ion−Molecule Reaction Dynamics. *Annu. Rev. Phys. Chem.* **2017**, *68*, 333−353.

(9) Li, J.; Zhao, B.; Xie, D.; Guo, H. Advances and New Challenges to Bimolecular Reaction Dynamics Theory. *J. Phys. Chem. Lett.* **2020**, *11*, 8844−8860.

(10) Czakó, G.; Győri, T.; Papp, D.; Tajti, V.; Tasi, D. A. First-Principles Reaction Dynamics beyond Six-Atom Systems. *J. Phys. Chem. A* **2021**, *125*, 2385−2393.

(11) Wester, R. Fifty Years of Nucleophilic Substitution in the Gas Phase. *Mass Spectrom. Rev.* **2022**, *41*, 627−644.

(12) Brauman, J. I. Not so Simple. *Science* **2008**, *319*, 168.

(13) Manikandan, P.; Zhang, J.; Hase, W. L. Chemical Dynamics Simulations of $X^- + CH_3Y \rightarrow XCH_3 + Y^-$ Gas-Phase S_N2 Nucleophilic Substitution Reactions. Nonstatistical Dynamics and Nontraditional Reaction Mechanisms. *J. Phys. Chem. A* **2012**, *116*, 3061−3080.

(14) Mikosch, J.; Zhang, J.; Trippel, S.; Eichhorn, C.; Otto, R.; Sun, R.; De Jong, W. A.; Weidemüller, M.; Hase, W. L.; Wester, R. Indirect Dynamics in a Highly Exoergic Substitution Reaction. *J. Am. Chem. Soc.* **2013**, *135*, 4250−4259.

(15) Xie, J.; Hase, W. L. Rethinking the S_N2 Reaction. *Science* **2016**, *352*, 32−33.

(16) Carrascosa, E.; Michaelsen, T.; Stei, M.; Bastian, B.; Meyer, J.; Mikosch, J.; Wester, R. Imaging Proton Transfer and Dihalide Formation Pathways in Reactions of $F^- + CH_3I$. *J. Phys. Chem. A* **2016**, *120*, 4711−4719.

(17) Szabó, I.; Czakó, G. Revealing a Double-Inversion Mechanism for the $F^- + CH_3Cl$ S_N2 Reaction. *Nat. Commun.* **2015**, *6*, 5972.

(18) Zhang, J.; Mikosch, J.; Trippel, S.; Otto, R.; Weidemüller, M.; Wester, R.; Hase, W. L. $F^- + CH_3I \rightarrow FCH_3 + I^-$ Reaction Dynamics. Nontraditional Atomistic Mechanisms and Formation of a Hydrogen-Bonded Complex. *J. Phys. Chem. Lett.* **2010**, *1*, 2747−2752.

(19) Stei, M.; Carrascosa, E.; Kainz, M. A.; Kelkar, A. H.; Meyer, J.; Szabó, I.; Czakó, G.; Wester, R. Influence of the Leaving Group on the Dynamics of a Gas-Phase S_N2 Reaction. *Nat. Chem.* **2016**, *8*, 151−156.

(20) Nacsa, A. B.; Tajti, V.; Czakó, G. Dynamics of the $Cl^- + CH_3I$ Reaction on a High-Level Ab Initio Analytical Potential Energy Surface. *J. Chem. Phys.* **2023**, *158*, 194306.

(21) Zhang, J.; Yang, L.; Xie, J.; Hase, W. L. Microsolvated $F^-(H_2O) + CH_3I$ S_N2 Reaction Dynamics. Insight into the Suppressed Formation of Solvated Products. *J. Phys. Chem. Lett.* **2016**, *7*, 660−665.

(22) Liu, X.; Xie, J.; Zhang, J.; Yang, L.; Hase, W. L. Steric Effects of Solvent Molecules on S_N2 Substitution Dynamics. *J. Phys. Chem. Lett.* **2017**, *8*, 1885−1892.

(23) Yang, L.; Liu, X.; Zhang, J.; Xie, J. Effects of Microsolvation on a S_N2 Reaction: Indirect Atomistic Dynamics and Weakened Suppression of Reactivity. *Phys. Chem. Chem. Phys.* **2017**, *19*, 9992−9999.

(24) Olasz, B.; Czakó, G. High-Level-Optimized Stationary Points for the $F^-(H_2O) + CH_3I$ System: Proposing a New Water-Induced Double-Inversion Pathway. *J. Phys. Chem. A* **2019**, *123*, 454−462.

(25) Bastian, B.; Michaelsen, T.; Li, L.; Ončák, M.; Meyer, J.; Zhang, D. H.; Wester, R. Imaging Reaction Dynamics of $F^-(H_2O)$ and $Cl^-(H_2O)$ with CH_3I. *J. Phys. Chem. A* **2020**, *124*, 1929−1939.

(26) Bastian, B.; Michaelsen, T.; Ončák, M.; Meyer, J.; Wester, R. $F^-(H_2O)+CH_3I$ ligand exchange reaction dynamics. *Chin. J. Chem. Phys.* **2020**, *33*, 210−216.

(27) Bastian, B.; Michaelsen, T.; Ončák, M.; Meyer, J.; Wester, R. Suppression of Low Product Kinetic Energies in Reactions of FHO^- and $Cl^-(H_2O)$ with CH_3I. *Int. J. Mass Spectrom.* **2021**, *462*, 116526.

(28) Lu, X.; Li, L.; Zhang, X.; Fu, B.; Xu, X.; Zhang, D. H. Dynamical Effects of S_N2 Reactivity Suppression by Microsolvation: Dynamics Simulations of the $F^-(H_2O) + CH_3I$ Reaction on a 21-Dimensional Potential Energy Surface. *J. Phys. Chem. Lett.* **2022**, *13*, 5253−5259.

(29) Zhang, J.; Lourderaj, U.; Addepalli, S. V.; De Jong, W. A.; Hase, W. L. Quantum Chemical Calculations of the $Cl^- + CH_3I \rightarrow CH_3Cl + I^-$ Potential Energy Surface. *J. Phys. Chem. A* **2009**, *113*, 1976−1984.

(30) Zhang, J.; Yang, L.; Sheng, L. Electronic Structure Theory Study of the Microsolvated $F^-(H_2O) + CH_3I$ S_N2 Reaction. *J. Phys. Chem. A* **2016**, *120*, 3613−3622.

(31) Szabó, I.; Czakó, G. Benchmark Ab Initio Characterization of the Complex Potential Energy Surface of the $Cl^- + CH_3I$ Reaction. *J. Phys. Chem. A* **2017**, *121*, 5748−5757.

(32) Olasz, B.; Szabó, I.; Czakó, G. High-Level Ab Initio Potential Energy Surface and Dynamics of the F⁻ + CH₃I S_N2 and Proton-Transfer Reactions. *Chem. Sci.* **2017**, *8*, 3164−3170.

(33) Czakó, G.; Győri, T.; Olasz, B.; Papp, D.; Szabó, I.; Tajti, V.; Tasi, D. A. Benchmark Ab Initio and Dynamical Characterization of the Stationary Points of Reactive Atom + Alkane and S_N2 Potential Energy Surfaces. *Phys. Chem. Chem. Phys.* **2020**, *22*, 4298−4312.

(34) Ji, X.; Zhao, C.; Xie, J. Investigating the Role of Halogen-Bonded Complexes in Microsolvated Y⁻(H₂O)_n + CH₃I S_N2 Reactions. *Phys. Chem. Chem. Phys.* **2021**, *23*, 6349−6360.

(35) Bento, A. P.; Sola, M.; Bickelhaupt, F. M. E2 and S_N2 Reactions of X⁻ + CH₃CH₂X (X = F, Cl); an Ab Initio and DFT Benchmark Study. *J. Chem. Theory Comput.* **2008**, *4*, 929−940.

(36) Wu, X.-P.; Sun, X.-M.; Wei, X.-G.; Ren, Y.; Wong, N.-B.; Li, W.-K. Exploring the Reactivity Trends in the E2 and S_N2 Reactions of X⁻ + CH₃CH₂Cl (X = F, Cl, Br, HO, HS, HSe, NH₂ PH₂, AsH₂, CH₃, SiH₃, and GeH₃). *J. Chem. Theory Comput.* **2009**, *5*, 1597−1606.

(37) Swart, M.; Solà, M.; Bickelhaupt, F. M. Density Functional Calculations of E2 and S_N2 Reactions: Effects of the Choice of Method, Algorithm, and Numerical Accuracy. *J. Chem. Theory Comput.* **2010**, *6*, 3145−3152.

(38) Zhao, Y.; Truhlar, D. G. Density Functional Calculations of E2 and S_N2 Reactions: Effects of the Choice of Density Functional, Basis Set, and Self-Consistent Iterations. *J. Chem. Theory Comput.* **2010**, *6*, 1104−1108.

(39) Carrascosa, E.; Meyer, J.; Zhang, J.; Stei, M.; Michaelsen, T.; Hase, W. L.; Yang, L.; Wester, R. Imaging Dynamic Fingerprints of Competing E2 and S_N2 Reactions. *Nat. Commun.* **2017**, *8*, 25.

(40) Vermeeren, P.; Hansen, T.; Grasser, M.; Silva, D. R.; Hamlin, T. A.; Bickelhaupt, F. M. S_N2 versus E2 Competition of F⁻ and PH₂⁻ Revisited. *J. Org. Chem.* **2020**, *85*, 14087−14093.

(41) Vermeeren, P.; Hansen, T.; Jansen, P.; Swart, M.; Hamlin, T. A.; Bickelhaupt, F. M. A Unified Framework for Understanding Nucleophilicity and Protophilicity in the S_N2/E2 Competition. *Chem.—Eur. J.* **2020**, *26*, 15538−15548.

(42) Gallegos, M.; Costales, A.; Martín Pendás, Á. Does Steric Hindrance Actually Govern the Competition between Bimolecular Substitution and Elimination Reactions? *J. Phys. Chem. A* **2022**, *126*, 1871−1880.

(43) Wu, X.; Bickelhaupt, F. M.; Xie, J. Solvent-Induced Dual Nucleophiles and the α-Effect in the S_N2 versus E2 Competition. *Phys. Chem. Chem. Phys.* **2024**, *26*, 11320−11330.

(44) Wolfe, S.; Mitchell, D. J.; Schlegel, H. B. Theoretical Studies of S_N2 Transition States. Substituent Effects. *Can. J. Chem.* **1982**, *60*, 1291−1294.

(45) Shaik, S. S. α- and β-Carbon Substituent Effect on S_N2 Reactivity. A Valence-Bond Approach. *J. Am. Chem. Soc.* **1983**, *105*, 4359−4367.

(46) Gstir, T.; Michaelsen, T.; Long, B. A.; Nacsa, A. B.; Ayasli, A.; Swaraj, D.; Zappa, F.; Trummer, F.; Ard, S. G.; Shuman, N. S.; et al. The Influence of Fluorination on the Dynamics of the F⁻ + CH₃CH₂I Reaction. *Phys. Chem. Chem. Phys.* **2023**, *25*, 18711−18719.

(47) Kost, D.; Aviram, K. S_N2 Transition State. 5. Effect of α-Substituents on S_N2 Reactivity and the S_N2−S_N1 Borderline Problem. A Molecular Orbital Approach. *J. Am. Chem. Soc.* **1986**, *108*, 2006−2013.

(48) Hop, C. E. C. A.; McMahon, T. B. Translational Energy Dependence of Gas-Phase Reactions of Halides with Halogenated Alkanes. *J. Phys. Chem.* **1991**, *95*, 10582−10586.

(49) Morris, R. A.; Viggiano, A. A. Kinetics of the Reactions of F⁻ with CF₃Br and CF₃I as a Function of Temperature, Kinetic Energy, Internal Temperature, and Pressure. *J. Phys. Chem.* **1994**, *98*, 3740−3746.

(50) Morris, R. A.; Viggiano, A.; Paulson, J. F. Reactivity of Gas-Phase Anions with Fully Halogenated Alkanes. *Int. Rev. Phys. Chem.* **1996**, *15*, 183−204.

(51) Pagliai, M.; Raugei, S.; Cardini, G.; Schettino, V. Car−Parrinello Molecular Dynamics of the S_N2 Reaction Cl⁻ + Cl₂CH₂. *Phys. Chem. Chem. Phys.* **2001**, *3*, 4870−4873.

(52) Bogdanov, B.; McMahon, T. B. Gas Phase S_N2 Reactions of Halide Ions with Trifluoromethyl Halides: Front- and Back-Side Attack vs. Complex Formation. *J. Phys. Chem. A* **2006**, *110*, 1350−1363.

(53) Le Vot, C.; Lemaire, J.; Pernot, P.; Heninger, M.; Mestdagh, H.; Louarn, E. Oxygen Anion (O⁻) and Hydroxide Anion (HO⁻) Reactivity with a Series of Old and New Refrigerants. *J. Mass Spectrom.* **2018**, *53*, 336−352.

(54) Mensa-Bonsu, G.; Tozer, D. J.; Verlet, J. R. R. Photoelectron Spectroscopic Study of I⁻·ICF₃: A Frontside Attack S_N2 Pre-Reaction Complex. *Phys. Chem. Chem. Phys.* **2019**, *21*, 13977−13985.

(55) Hine, J.; Thomas, C. H.; Ehrenson, S. J. The Effect of Halogen Atoms on the Reactivity of Other Halogen Atoms in the Same Molecule. V. The S_N2 Reactivity of Methylene Halides. *J. Am. Chem. Soc.* **1955**, *77*, 3886−3889.

(56) Pagliai, M.; Raugei, S.; Cardini, G.; Schettino, V. Ab-Initio Molecular Dynamics Study of The S_N2 Reaction Cl⁻+ ClCH₂CN. *Phys. Chem. Chem. Phys.* **2001**, *3*, 2559−2566.

(57) Morris, R. A. Gas-phase Reactions of Oxide and Superoxide Anions with CF₄, CF₃Cl, CF₃Br, CF₃I, and C₂F₄ at 298 and 500 K. *J. Chem. Phys.* **1992**, *97*, 2372−2381.

(58) Morris, R. A.; Viggiano, A. A.; Arnold, S. T.; Paulson, J. F.; Liebman, J. F. Reactions of Atmospheric Ions with Selected Hydrofluorocarbons. *J. Phys. Chem.* **1995**, *99*, 5992−5999.

(59) Morris, R. A.; Viggiano, A. A.; Miller, T. M.; Seeley, J. V.; Arnold, S. T.; Paulson, J. F.; Van Doren, J. M. Reactivity of Negative Ions with Trifluoromethyl Halides. *J. Phys. Chem.* **1996**, *100*, 10641−10645.

(60) Xie, J.; McClellan, M.; Sun, R.; Kohale, S. C.; Govind, N.; Hase, W. L. Direct Dynamics Simulation of Dissociation of the [CH₃−I−OH]⁻ Ion−Molecule Complex. *J. Phys. Chem. A* **2015**, *119*, 817−825.

(61) Meyer, J.; Tajti, V.; Carrascosa, E.; Győri, T.; Stei, M.; Michaelsen, T.; Bastian, B.; Czakó, G.; Wester, R. Atomistic Dynamics of Elimination and Nucleophilic Substitution Disentangled for the F⁻ + CH₃CH₂Cl Reaction. *Nat. Chem.* **2021**, *13*, 977−981.

(62) Tasi, D. A.; Michaelsen, T.; Wester, R.; Czakó, G. Quasi-Classical Trajectory Study of the OH⁻ + CH₃I Reaction: Theory Meets Experiment. *Phys. Chem. Chem. Phys.* **2023**, *25*, 4005−4014.

(63) Møller, C.; Plesset, M. S. Note on an Approximation Treatment for Many-Electron Systems. *Phys. Rev.* **1934**, *46*, 618−622.

(64) Dunning, T. H. Gaussian Basis Sets for Use in Correlated Molecular Calculations. I. The Atoms Boron through Neon and Hydrogen. *J. Chem. Phys.* **1989**, *90*, 1007−1023.

(65) Adler, T. B.; Knizia, G.; Werner, H. J. A Simple and Efficient CCSD(T)-F12 Approximation. *J. Chem. Phys.* **2007**, *127*, 221106.

(66) Raghavachari, K.; Trucks, G. W.; Pople, J. A.; Head-Gordon, M. A. A fifth-order perturbation comparison of electron correlation theories. *Chem. Phys. Lett.* **1989**, *157*, 479−483.

(67) Noga, J.; Bartlett, R. J. The Full CCSDT Model for Molecular Electronic Structure. *J. Chem. Phys.* **1987**, *86*, 7041−7050.

(68) Kállay, M.; Gauss, J. Approximate Treatment of Higher Excitations in Coupled-Cluster Theory. *J. Chem. Phys.* **2005**, *123*, 214105.

(69) Peterson, K. A.; Dunning, T. H. Accurate Correlation Consistent Basis Sets for Molecular Core−Valence Correlation Effects: The Second Row Atoms Al−Ar, and the First Row Atoms B−Ne Revisited. *J. Chem. Phys.* **2002**, *117*, 10548−10560.

(70) Peterson, K. A.; Figgen, D.; Goll, E.; Stoll, H.; Dolg, M. Systematically Convergent Basis Sets with Relativistic Pseudopotentials. II. Small-Core Pseudopotentials and Correlation Consistent Basis Sets for the Post-d Group 16−18 Elements. *J. Chem. Phys.* **2003**, *119*, 11113−11123.

(71) Werner, H. J.; Manby, F. R.; Knowles, P. J. Fast Linear Scaling Second-Order Møller-Plesset Perturbation Theory (MP2) Using Local and Density Fitting Approximations. *J. Chem. Phys.* **2003**, *118*, 8149−8160.

(72) Werner, H. J.; Adler, T. B.; Manby, F. R. General Orbital Invariant MP2-F12 Theory. *J. Chem. Phys.* **2007**, *126*, 164102.

(73) Werner, H.-J.; Knowles, P. J.; Knizia, G.; Manby, F. R.; Schütz, M.; Celani, P.; Győrffy, W.; Kats, D.; Korona, T.; Lindh, R.; et al. *Molpro*, version 2015.1, a package of ab initio programs, 2024. http://www.molpro.net (accessed 18 October 2024).

(74) Kállay, M.; Nagy, P. R.; Mester, D.; Rolik, Z.; Samu, G.; Csontos, J.; Csóka, J.; Szabó, P. B.; Gyevi-Nagy, L.; Hégely, B.; et al. The MRCC Program System: Accurate Quantum Chemistry from Water to Proteins. *J. Chem. Phys.* **2020**, *152*, 074107.

(75) Kállay, M.; Nagy, P. R.; Mester, D.; Rolik, Z.; Samu, G.; Csontos, J.; Csóka, J.; Szabó, P. B.; Gyevi-Nagy, L.; Hégely, B. *MRCC, a quantum chemical program suite*, 2024. www.mrcc.hu (accessed 18 October 2024).

(76) Tasi, D. A.; Fábián, Z.; Czakó, G. Benchmark Ab Initio Characterization of the Inversion and Retention Pathways of the OH^- + CH_3Y [Y = F, Cl, Br, I] S_N2 Reactions. *J. Phys. Chem. A* **2018**, *122*, 5773−5780.

(77) Tasi, D. A.; Fábián, Z.; Czakó, G. Rethinking the X^- + CH_3Y [X = OH, SH, CN, NH_2, PH_2; Y = F, Cl, Br, I] S_N2 Reactions. *Phys. Chem. Chem. Phys.* **2019**, *21*, 7924−7931.

(78) Tasi, D. A.; Czakó, G. Benchmark Ab Initio Characterization of the Complex Potential Energy Surfaces of the HOO^- + CH_3Y [Y = F, Cl, Br, I] Reactions. *Phys. Chem. Chem. Phys.* **2024**, *26*, 16048−16059.